Development 140, 1240-1249 (2013) doi:10.1242/dev.087874

The ETS domain transcriptional repressor Anterior open inhibits MAP kinase and Wingless signaling to couple tracheal cell fate with branch identity

Sara Caviglia* and Stefan Luschnig*

SUMMARY

Cells at the tips of budding branches in the *Drosophila* tracheal system generate two morphologically different types of seamless tubes. Terminal cells (TCs) form branched lumenized extensions that mediate gas exchange at target tissues, whereas fusion cells (FCs) form ring-like connections between adjacent tracheal metameres. Each tracheal branch contains a specific set of TCs, FCs, or both, but the mechanisms that select between the two tip cell types in a branch-specific fashion are not clear. Here, we show that the ETS domain transcriptional repressor *anterior open* (*aop*) is dispensable for directed tracheal cell migration, but plays a key role in tracheal tip cell fate specification. Whereas *aop* globally inhibits TC and FC specification, MAPK signaling overcomes this inhibition by triggering degradation of Aop in tip cells. Loss of *aop* function causes excessive FC and TC specification, indicating that without Aop-mediated inhibition, all tracheal cells are competent to adopt a specialized fate. We demonstrate that Aop plays a dual role by inhibiting both MAPK and Wingless signaling, which induce TC and FC fate, respectively. In addition, the branch-specific choice between the two seamless tube types depends on the tracheal branch identity gene *spalt major*, which is sufficient to inhibit TC specification. Thus, a single repressor, Aop, integrates two different signals to couple tip cell fate selection with branch identity. The switch from a branching towards an anastomosing tip cell type may have evolved with the acquisition of a main tube that connects separate tracheal primordia to generate a tubular network.

KEY WORDS: *Drosophila melanogaster*, *anterior open*, Yan, TEL1, ETS domain, MAPK, Wingless, *spalt*, Tracheal system, Epithelial tube morphogenesis, Angiogenesis, Tip cell specification

INTRODUCTION

Tip cells are specialized endothelial cells that lead the migration of sprouting vessels and mediate anastomosis formation during vascular development in vertebrates (Geudens and Gerhardt, 2011; Herwig et al., 2011). Signaling through Vascular endothelial growth factor receptor (VEGFR), a receptor tyrosine kinase (RTK), is involved in selecting tip cells and in guiding their directed migration. However, the mechanisms that select between different tip cell behaviors (migration versus anastomosis formation) are not clear. In the *Drosophila* tracheal system, 20 groups of epidermal cells generate a tubular network through a sequence of branching and tube fusion events (Ghabrial et al., 2003; Uv et al., 2003; Affolter and Caussinus, 2008; Maruyama and Andrew, 2012). Tracheal cells invaginate from the epidermis and subsequently migrate in a stereotyped pattern guided by the local expression of the Fibroblast growth factor (FGF) homolog Branchless (Bnl) (Sutherland et al., 1996). Bnl activates the FGF receptor (FGFR) Breathless (Btl) on tracheal tip cells, which lead the concerted migration towards the Bnl source. Reminiscent of the role of VEGFR signaling in angiogenesis, Bnl promotes and guides cell motility, but also stimulates differentiation of tracheal tip cells through activating Ras-MAPK signaling (Samakovlis et al., 1996a; Samakovlis et al., 1996b). Whereas the branch stalk cells form tubes with extracellular lumina sealed by cell-cell junctions, tip cells generate two different types of seamless tubes with intracellular lumina. Terminal cells (TCs), which express the *Drosophila* Serum response factor homolog (DSRF; Bs – FlyBase) (Guillemin et al., 1996; Montagne et al., 1996) under the control of Ras-MAPK signaling, develop branched and lumenized cytoplasmic extensions that mediate gas exchange at the target tissues. The second type of seamless tubes, generated by fusion cells (FCs), mediates the connection of adjacent tracheal metameres. A single FC expressing the Zn-finger protein Escargot (Esg) (Samakovlis et al., 1996b; Tanaka-Matakatsu et al., 1996) and the bHLH protein Dysfusion (Dys) (Jiang and Crews, 2003) is specified at the tip of each branch that will connect with a cognate branch from a neighboring or contralateral tracheal metamere. FC specification involves FGF signaling and branch-specific Wingless (Wg) and TGFβ signals, which promote the FC fate (Steneberg et al., 1999; Chihara and Hayashi, 2000; Llimargas, 2000). Conversely, Delta/Notch-dependent lateral inhibition prevents neighboring cells from assuming FC fate, thus ensuring that a single FC is specified at each branch tip (Ikeya and Hayashi, 1999; Llimargas, 1999). Although high-level MAPK activation in tip cells promotes both FC and TC specification, the choice between the two tip cell fates is regulated in a branch-specific fashion. The tips of most tracheal branches contain a single FC and at least one TC. However, the main longitudinal dorsal trunk (DT) tube contains only FCs, whereas the visceral branches (VB), which originate from the same region as the DT, contain only TCs. Although the correct choice between the two different seamless tube types is essential for the formation of a functional respiratory network, how tip cell fate choice is coordinated with branch identity remains unclear. It has been shown that DT identity and FC specification in the DT depend on Wg signaling (Chihara and Hayashi, 2000; Llimargas, 2000), but how

Institute of Molecular Life Sciences and PhD Program in Molecular Life Sciences, University of Zurich, Winterthurer Str. 190, CH-8057 Zurich, Switzerland.

*Authors for correspondence (sara.caviglia@imls.uzh.ch; stefan.luschnig@imls.uzh.ch)

Accepted 2 January 2013

Wg and MAPK signals are integrated within tip cells to control FC specification is not known.

We show here that the ETS domain transcriptional repressor Anterior open (Aop; also known as Yan) (Lai and Rubin, 1992; Tei et al., 1992) plays a key role in the region-specific selection of tip cell fate in the tracheal system. Aop blocks signaling downstream of different RTKs by competing with the ETS domain transcriptional activator Pointed (Pnt) for binding to shared *cis*-regulatory elements (Rebay, 2002). Phosphorylation by MAPK activates Pnt and inactivates Aop, thus resulting in target gene activation (Brunner et al., 1994). Interestingly, Aop was recently found to repress not only RTK signaling, but also Wg signaling in the developing *Drosophila* eye, possibly through interacting with Armadillo (Arm) (Olson et al., 2011). We show that Aop acts in a dual fashion by inhibiting both MAPK-dependent TC specification and Wg-dependent FC specification in tracheal non-tip cells. In the absence of *aop* function, every tracheal cell is able to adopt a specialized (TC or FC) fate. We show that the choice between the two fates is determined not only by the nature of the inducers (Wg or Bnl), but it is constrained by factors that define tracheal branch identity: expression of the selector gene *spalt major* (*salm*) biases the competence of tracheal tip cells towards FC fate. Thus, a single transcriptional repressor, Aop, integrates two different signals to couple tip cell fate selection with tracheal branch identity.

MATERIALS AND METHODS

Drosophila strains

The aop^{O199} mutation was isolated in an ethyl methanesulfonate mutagenesis screen (Förster et al., 2010). Unless otherwise mentioned, *Drosophila* stocks were obtained from the Bloomington Stock Center: *Df(2L)BSC688*, *69B*-Gal4, *UAS-mCherry-NLS*, *UAS-GFP* (FlyBase), *UAS-Verm-mRFP* (Förster et al., 2010), *btl*-Gal4 (Shiga et al., 1996), $esg\text{-}LacZ^{B7\text{-}2\text{-}22}$ (Samakovlis et al., 1996b), aop^{1}, $salm^{1}$ (Nusslein-Volhard et al., 1984), pnt^{A88} (Brunner et al., 1994), sty^{226} (Kramer et al., 1999), *UAS-aop*, $UAS\text{-}Aop^{ACT}$ (Rebay and Rubin, 1995), *UAS-dys*, *dys*C1.7::nlsGFP (Jiang et al., 2010), *E-Cad-mTomato* (Huang et al., 2009), *UAS-bnl* (Sutherland et al., 1996), *UAS-λBtl* (Lee et al., 1996), *UAS-λTop* (Queenan et al., 1997), $UAS\text{-}arm^{S10}$ (Pai et al., 1997), UAS-dnTCF (*UAS-dTCFΔN-HA*) (van de Wetering et al., 1997), *UAS-Axin-GFP* (Cliffe et al., 2003) and *UAS-salm* (Kühnlein and Schuh, 1996).

Sequencing of *aop* alleles

Homozygous aop^{O199} and aop^{1} embryos were selected by the absence of the *CyO Dfd-YFP* balancer chromosome (Le et al., 2006). Genomic DNA was extracted from 15 embryos. The *aop* locus was amplified by PCR with oligonucleotides SC1 (5′-GTTTTCCGTTTCGATTGCAT) and SC2 (5′-CTGACCGGGACAATTCCTTA). PCR products were sequenced on both strands.

Immunostainings

Embryos were fixed in 4% formaldehyde for 20 minutes and devitellinized by shaking in methanol/heptane. Primary antibodies (mouse anti-GFP, rabbit anti-GFP, rabbit anti-mCherry) were used as previously described (Förster et al., 2010). Other antibodies used were mouse anti-Aop 8B12H9 (1:10; (Rebay and Rubin, 1995), mouse anti-Arm N27A1 (1:7, DSHB), rabbit anti-β-Galactosidase (1:1000; Cappel), mouse anti-Delta extracellular domain C594.9B (1:100; DSHB), mouse anti-DSRF (1:300; Samakovlis et al., 1996b), rabbit anti-Dys (1:500; Jiang and Crews, 2003), mouse-anti-GFP (1:500; Roche), rat anti-HA 3F10 (1:300; Roche), rabbit anti-Salm (1:40; Kühnlein and Schuh, 1996) and guinea pig anti-Uif (1:1000; Zhang and Ward, 2009). Goat secondary antibodies were conjugated with AlexaFluor 488, 559 (Molecular Probes) or Cy5 (Jackson ImmunoResearch). Chitin was detected using SNAP-tagged chitin-binding domain from chitinase A1 of *Bacillus circulans* (plasmid provided by Yinhua Zhang, New England Biolabs) (Watanabe et al., 1994), which was expressed as a His-tagged protein in *E. coli*, purified using Nickel-NTA sepharose and labeled with SNAP-Surface AlexaFluor 425, 488, 546 or 647 (New England Biolabs).

Imaging and quantifications

Specimens were imaged using an Olympus FV1000 confocal microscope. For live imaging, staged embryos were dechorionated, glued on a coverslip and immersed in Voltalef 10S oil. *Z*-stacks (0.5-1.5 μm step size) were projected using Imaris (v7.3.1, Bitplane) or Fiji (GPL v2). The Imaris oblique slicer tool was used to create virtual projections (1-3 μm thick) oriented in *yz* (Fig. 1C′,D′; Fig. 2C′,E′) or *xy* (Fig. 4L′,M′). For FC and TC quantification, Dys- or DSRF-positive nuclei in the DT (Tr1-10), DB (Tr1-10), LT ($LT_pTr1\text{-}LT_aTr10$) and GB (Tr1-10) were counted using the spot tool in Imaris. At least seven embryos per genotype were analyzed. To calculate average TC and FC numbers per branch tip, the total number of TCs or FCs found in each branch type was divided by the number of branch tips that were scored in a given embryo. *P* values were calculated using two-tailed, unpaired Student's *t*-test. Salm protein levels were measured in aop^{0199} and *btl-Gal4; UAS-*Aop^{ACT} embryos, which were co-stained with wild-type control embryos in the same reaction. Nuclei of tracheal cells in DT metameres Tr8-9 were segmented using the Imaris spot tool. Mean intensities from a total of at least 200 nuclei from at least seven embryos per genotype were averaged. Average values from wild-type controls for each genotype were set to 100% to calculate fold change values. Standard deviations were calculated from the mean of normalized values. *P* values were calculated using two-tailed, unpaired Student's *t*-test.

RESULTS

O199 mutants show cellular inclusions within the tracheal lumen

We isolated a new class of embryonic lethal mutants showing abnormally shaped tracheal tubes. In one such mutant, *O199*, the tracheal branching pattern was normal, but the lumen of the DT showed apparent 'holes' where luminal material was excluded (Fig. 1A,B). These structures were variable in size and occurred mainly within metameres 5-9 near to DT fusion joints (data not shown). The exclusion of luminal material was due to cellular bridges traversing the DT lumen (Fig. 1C,D). Time-lapse imaging revealed the origin of these structures (Fig. 1E,F; supplementary material Movie 1). After completion of DT fusion, the lumen began to bend towards one side, leading to a local indentation. Shortly afterwards, two fine luminal extensions invaded the indentation from both sides and subsequently joined, giving rise to a secondary lumen separated from the original lumen by a cellular bridge.

O199 is a loss-of-function mutation in the ETS domain transcriptional repressor *anterior open*

We mapped the *O199* mutation to the *aop* locus (Lai and Rubin, 1992; Tei et al., 1992). Tracheal defects of aop^{O199} homozygotes were similar to those of $aop^{O199}/Df(2L)BSC688$ hemizygous embryos (supplementary material Fig. S1), indicating that *O199* is an amorphic *aop* allele. *O199* failed to complement the aop^{1} mutation (Nusslein-Volhard et al., 1984; Rogge et al., 1995) and aop^{1} embryos showed tracheal defects resembling those of *O199* mutants (data not shown). Sequence analysis revealed that aop^{1} carries a premature stop codon resulting in a predicted truncated protein lacking the ETS DNA-binding domain (Fig. 1G,H). *O199* carries a 203 bp deletion in the first coding exon, resulting in a frame shift and a predicted protein that is truncated after the Pointed (PNT) domain. Aop protein was not detectable in aop^{O199} embryos (supplementary material Fig. S2). Tracheal-specific expression of an *aop* cDNA (Rebay and Rubin, 1995) completely rescued the tracheal defects of aop^{O199} mutants (supplementary material Fig. S1). We conclude that aop^{O199} is an *aop* loss-of-function allele and that *aop* function is required in tracheal cells for the normal shape of the DT lumen.

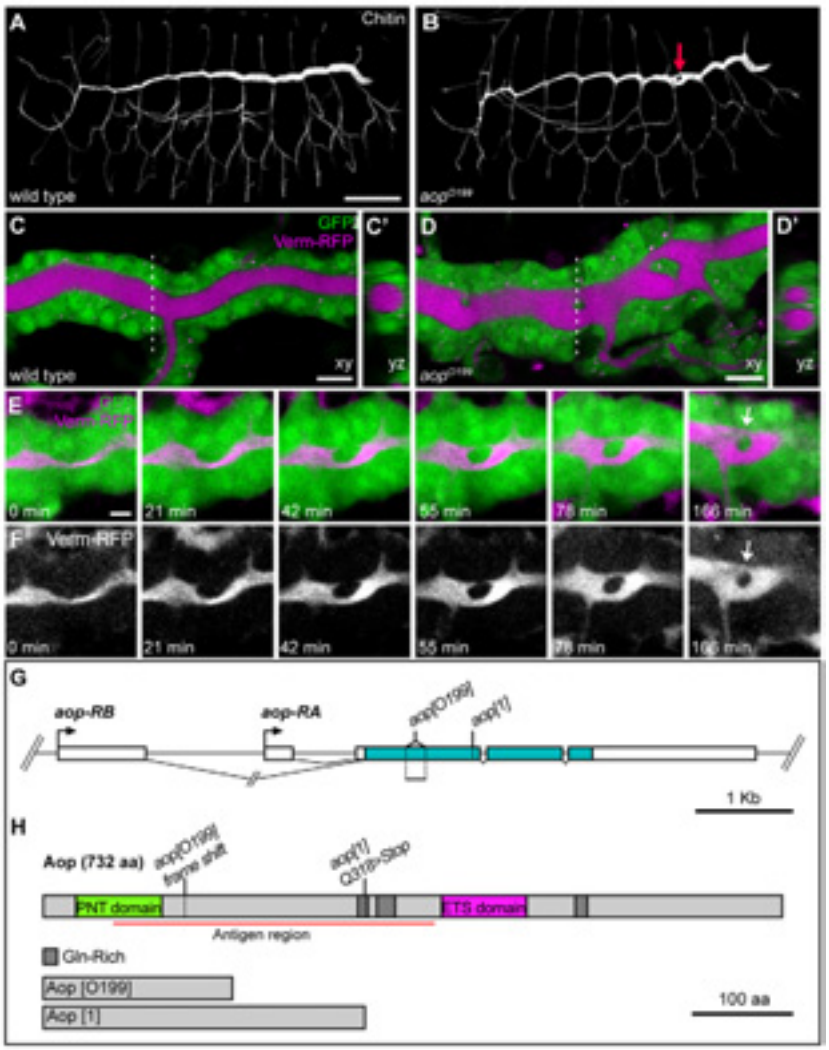

Fig. 1. *aop*^{O199} mutants show cellular inclusions within the dorsal trunk lumen. (**A**,**B**) Stage 15 wild-type (A) and *aop*^{O199} (B) embryos stained for chitin. Tracheal architecture is normal in *aop*^{O199} embryos, but local exclusions of luminal material are visible in the DT (arrow in B). (**C-D′**) Confocal sections of DT in living wild-type (C,C′) and *aop*^{O199} (D,D′) embryos expressing GFP (green) and Verm-mRFP (magenta). Notice the cellular inclusions in the DT lumen of the *aop*^{O199} embryo. Broken lines indicate planes of cross-sections shown in C′ and D′. (**E**,**F**) Time-lapse imaging of DT in an *aop*^{O199} embryo shows that cellular inclusions result from the formation of secondary lumina (arrows). Lumen is labeled using Verm-mRFP (F; magenta in E). Time 0 is 12 hours after egg lay (see supplementary material Movie 1). (**G**,**H**) Structure of the *aop* locus (G) and of Aop protein (H). *aop*^{O199} carries a 203 bp deletion (starting at C420 in the coding sequence of the cDNA) in the first coding exon that leads to a frame shift. *aop*^{1} carries a premature stop codon (G952A). The *aop*^{O199} and *aop*^{1} mutations lead to predicted truncated proteins that lack the ETS DNA-binding domain (H). The region containing the epitope recognized by the anti-Aop monoclonal antibody is marked. Scale bars: 50 μm in A,B; 10 μm in C-F.

Luminal bifurcations in *aop* mutants are due to extra tracheal fusion events

We hypothesized that the formation of secondary lumina in the DT of *aop* mutants could result from extra tracheal fusion events. Wild-type embryos contain a single Dys-positive FC per branch tip (Fig. 2A). By contrast, *aop*^{O199} mutants showed extra (2.8±0.3 per tip) Dys-positive cells in the DT (Fig. 2B). Like wild-type FCs, every Dys::nls-GFP-positive cell in *aop*^{O199} mutants showed elevated levels of E-Cadherin-mTomato (E-Cad-mTomato) at adherens junctions (AJs; Fig. 2C-F) (Tanaka-Matakatsu et al., 1996). At least four FCs were located adjacent to the luminal bifurcations in *aop*^{O199} mutants. Tube cross-sections of such sites revealed two adjacent triple-ring-shaped AJs, characteristic of FC toroids, flanking the separated part of the lumen (Fig. 2E,F). Thus, DT cells in *aop*^{O199} become mis-specified as FCs. These supernumerary FCs undergo morphological transformations that are characteristic of wild-type FCs and they accomplish extra fusion events, which result in the formation of luminal bifurcations.

MAPK signaling promotes specification of tracheal fusion cells and terminal cells in a complementary pattern

Interestingly, supernumerary FCs in *aop* mutants were limited to the DT, whereas in all other branches numbers and positions of FCs were normal (Fig. 2G,I,K). However, *aop* mutants showed many extra TCs, as detected by DSRF expression in dorsal branches (DB), VB, lateral trunk (LT) and ganglionic branches (GB), but not in the DT (Fig. 2H,J,L). These supernumerary TCs gave rise to additional terminal ramifications, reminiscent of mutations in *sprouty* (*sty*), a negative regulator of MAPK signaling (Hacohen et al., 1998). Notably, *sty* mutants showed supernumerary FCs and TCs in the same complementary pattern as in *aop* mutants (supplementary material Fig. S1). These results suggest that negative regulation of MAPK signaling through *aop* and *sty* prevents ectopic specification of FCs and TCs, respectively, in distinct, non-overlapping regions of the tracheal system.

aop function is dispensable for tracheal cell migration and branching morphogenesis

Interestingly, despite the dramatic effect on FC and TC specification, the tracheal branching pattern was unaffected in *aop* mutants (Fig. 1B), suggesting that *aop* is dispensable for directed tracheal cell migration. We therefore monitored the appearance of FCs and TCs in *aop* mutants (Fig. 3A-F). Supernumerary Dys-expressing cells were first detectable in the DT during tracheal branch outgrowth at stage 13, slightly after Dys expression appeared in the regular FCs at DT fusion points (Fig. 3B). The number of extra FCs increased during later stages, possibly reflecting the

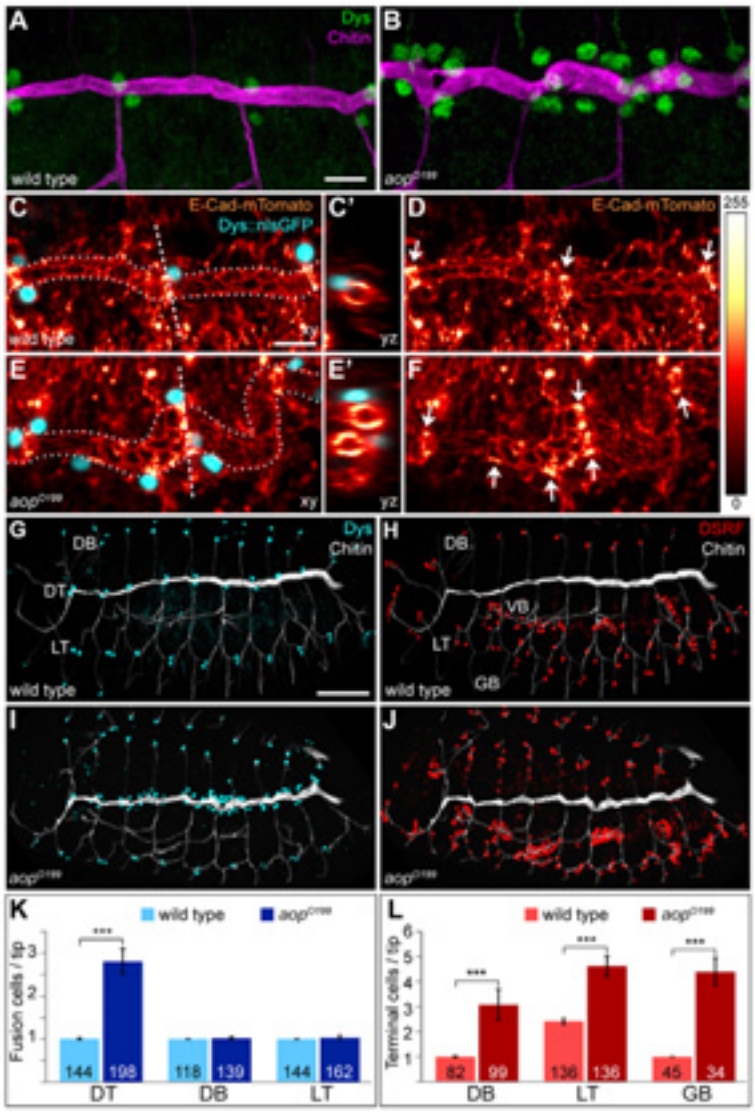

Fig. 2. *aop* mutations lead to ectopic specification of fusion cells and terminal cells in a complementary pattern. (**A**) Wild-type embryos contain two FCs labeled by nuclear Dysfusion (Dys, green) staining at each DT fusion joint. (**B**) aop^{O199} embryos contain extra Dys-positive cells distributed throughout DT metameres. Luminal chitin is labeled in magenta. (**C-F**) Living stage 15 wild-type (C-D) and aop^{O199} (E-F) embryos expressing Dys::nlsGFP (cyan) and E-Cad-mTomato (signal intensities displayed as a heat map). E-Cad levels are elevated in all Dys-positive cells in aop^{O199} mutants (D,F, arrows). (C′,E′) Cross-sections taken at the levels of the broken lines reveal a single ring-shaped adherens junction at the wild-type fusion joint (C′), whereas two separate rings are visible in the aop^{O199} mutant (E′), indicating that two fusion events took place. DT lumen is outlined by a dotted line in C,E. (**G-J**) Wild-type (G,H) and aop^{O199} (I,J) embryos stained with FC- (Dys, cyan) and TC- (DSRF, red) specific markers. aop^{O199} embryos show supernumerary FCs in the DT, but not in other branches. Conversely, supernumerary TCs are present in dorsal branches (DB), lateral trunks (LT) and ganglionic branches (GB), but not in the DT. (**K**,**L**) Quantification of FC and TC number in wild-type and aop^{O199} embryos. Branch types are indicated below the bars. Numbers inside bars indicate numbers of branch tips scored. Error bars represent s.d. ***$P \leq 0.001$. Scale bars: 10 μm in A-F; 50 μm in G-J.

depletion of maternal *aop* gene products (Fig. 3C). Extra DSRF-positive TCs were detectable in the DB, LT, and GB during the extension of these branches in stage 14 (Fig. 3D-G). Together, these findings suggest that directed cell migration can proceed normally in the presence of multiple ectopic tip cell-like cells distributed throughout the tracheal primordium.

aop prevents tracheal cells from assuming fusion or terminal cell fate

To understand how Aop blocks FC and TC differentiation, we examined Aop protein distribution during tracheal development. Although Aop is expressed throughout the tracheal system, Aop protein levels change dynamically with peak levels at stage 14 (supplementary material Fig. S2) (Lai and Rubin, 1992). At this stage, Aop is detectable in all tracheal nuclei, except in the tip cells of each branch, where MAPK signaling triggers Aop degradation (Fig. 3H-K) (Ohshiro et al., 2002). Expression of FC and TC markers (Dys, DSRF) coincides with the absence of Aop from the tip cells (supplementary material Fig. S3) (data not shown). Consistent with a role of Aop in blocking differentiation, expression of a constitutively active non-phosphorylatable form of Aop (UAS-Aop^{ACT}) (Rebay and Rubin, 1995) in all tracheal cells prevents them from assuming either FC or TC fate (Fig. 3L,M). Aop^{ACT} expression also suppressed the formation of supernumerary FCs and TCs in *sty* mutants, consistent with the notion that *sty* negatively regulates RTK signaling upstream of *aop* (supplementary material Fig. S1) (Hacohen et al., 1998; Kramer et al., 1999). These findings suggest that MAPK signaling triggers FC and TC differentiation by inducing Aop degradation, whereas the region-specific choice between FC and TC fates depends on additional instructive signals.

EGFR and Btl/FGFR have distinct capacities in inducing fusion cells and terminal cells

To uncover the nature of these signals, we examined factors that subdivide the tracheal primordium into distinct regions. Epidermal growth factor receptor (EGFR) and Wg signaling act in the central region, which will give rise to the DT (Wappner et al., 1997; Chihara and Hayashi, 2000; Llimargas, 2000). Conversely, Btl is initially expressed in all tracheal cells, but subsequently declines in the central region (Ohshiro et al., 2002). Given the distinct spatiotemporal patterns of Btl/FGFR and EGFR in the tracheae, we asked whether the two receptors differ in their capacity to induce FC and TC differentiation, respectively. To test this idea, we expressed in all tracheal cells constitutively active forms of either Btl (λBtl) (Lee et al.,

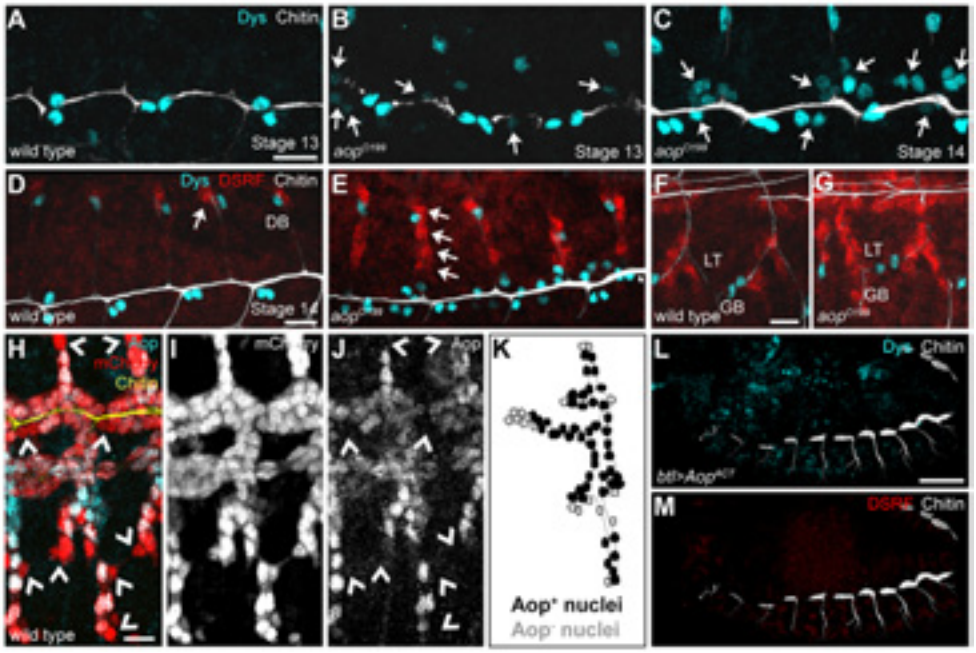

Fig. 3. Aop inhibits specification of fusion cells and terminal cells. (**A-C**) In wild-type embryos, Dys-positive FCs are detectable at the tips of migrating DT branches during stage 12 (not shown) and show high Dys levels by stage 13 (A). In *aop*^{O199} embryos (B,C) the regular set of FCs show high Dys levels at stage 13, whereas ectopic FCs (arrows in B) show lower Dys levels. Ectopic FCs show high Dys levels at stage 14 (C, arrows), when DT migration is nearly complete. (**D-G**) In wild-type embryos, DSRF-positive TCs are detectable at tips of DB (D, arrow), LT and GB (F) at stage 14. In *aop*^{O199} embryos, both regular and ectopic DSRF-positive TCs are detected at stage 14 in DB (E, arrows), LT and GB (G) branches, which are still migrating. (**H-J**) Stage 14 embryos expressing mCherry-NLS (I, red in H) in all tracheal cells were stained for Aop (J, cyan in H). Nuclear accumulation of Aop is abolished in all tip cells (arrowheads). (**K**) Tracheal metamere five schematic showing the positions of Aop-positive (black) and Aop-negative (gray) nuclei. (**L**,**M**) Tracheal expression of non-degradable Aop (Aop^{ACT}) inhibits specification of FCs (L) and TCs (M) at every branch tip. Scale bars: 10 μm in A-J; 50 μm in L,M.

1996) or EGFR (λTop) (Queenan et al., 1997) and counted FCs and TCs. As previously shown, λBtl efficiently induced extra TCs in the DB, LT and GB (supplementary material Fig. S3) (Lee et al., 1996), whereas λTop was significantly less effective than λBtl in inducing TCs (supplementary material Fig. S3; Fig. 2H) (Dossenbach et al., 2001). Strikingly, however, λTop was clearly more effective than λBtl in inducing extra FCs in the DT (supplementary material Fig. S3; Fig. 2G). Aop levels in λTop-expressing cells were lower than in λBtl-expressing cells (supplementary material Fig. S3), suggesting that λTop causes more efficient degradation of Aop, probably through stronger MAPK activation. Together, these results suggest that qualitative differences in signaling downstream of the two receptors may contribute to their different potential in TC specification, but that these differences are not sufficient to explain the branch-specific choice between TC and FC induction.

Aop blocks fusion cell induction in the dorsal trunk by antagonizing Wingless signaling

Besides RTK signaling, Wingless (Wg) signaling is necessary and sufficient to induce FCs in the DT by activating transcription of FC-specific genes, including *esg* and *Delta* (Chihara and Hayashi, 2000; Llimargas, 2000). To test whether *aop* might interfere with Wg signaling, we analyzed the expression of Wg target genes in *aop* mutant embryos (Fig. 4A-H; supplementary material Fig. S4). Notably, levels of Delta protein in the DT were increased in *aop* mutants compared with wild-type controls (Fig. 4A,B). Conversely, Delta levels were strongly reduced in the DT of Aop^{ACT}-expressing embryos (Fig. 4C). Similar to Delta, the expression of an *esg-LacZ* reporter gene was markedly increased in *aop* mutants compared with wild-type controls, and was absent from Aop^{ACT}-expressing tracheal cells (supplementary material Fig. S4). Furthermore, levels of Salm protein, the expression of which in tracheal cells depends on Wg signaling (Llimargas, 2000), were increased by 20% in the DT of *aop* mutants (Fig. 4E,F) and decreased by 30% in embryos expressing Aop^{ACT} (Fig. 4G,H). Finally, we analyzed the distribution of the Wg signaling effector Arm in *aop* mutants. Although Arm levels at AJs were similar in *aop* and wild-type embryos (data not shown), *aop* mutants showed conspicuous accumulations of Arm in the cytoplasm and in intracellular punctae (supplementary material Fig. S4). Together, these findings suggest that *aop* negatively impacts on Wg signaling and consequently Wg target gene expression in tracheal cells. Consistent with this idea, Aop was recently shown to antagonize Wg signaling during *Drosophila* eye development (Olson et al., 2011). To corroborate that Aop also antagonizes Wg signaling in tracheal cells, we expressed in all tracheal cells a constitutively active form of Arm (Arm^{S10}), which led to the specification of supernumerary FCs in the DT, transverse connective branch, VB and LT (Fig. 4I) (Chihara and Hayashi, 2000; Llimargas, 2000), while TC specification remained largely normal (Fig. 4J). Interestingly, in all Arm^{S10}-induced FCs Aop was undetectable, suggesting that absence of Aop is necessary for FC induction through Wg signaling (Fig. 4K-M). To test whether FC mis-specification in *aop* mutants is due to deregulated Wg signaling, we blocked Wg-induced transcriptional activation by expressing a dominant-negative form of TCF (dTCFΔN) (van de Wetering et al., 1997) in tracheal cells. dTCFΔN expression led to a partial loss of FCs in the DT and to DT fusion defects (Fig. 4N,O) (Llimargas, 2000). Strikingly, in *aop*^{O199}

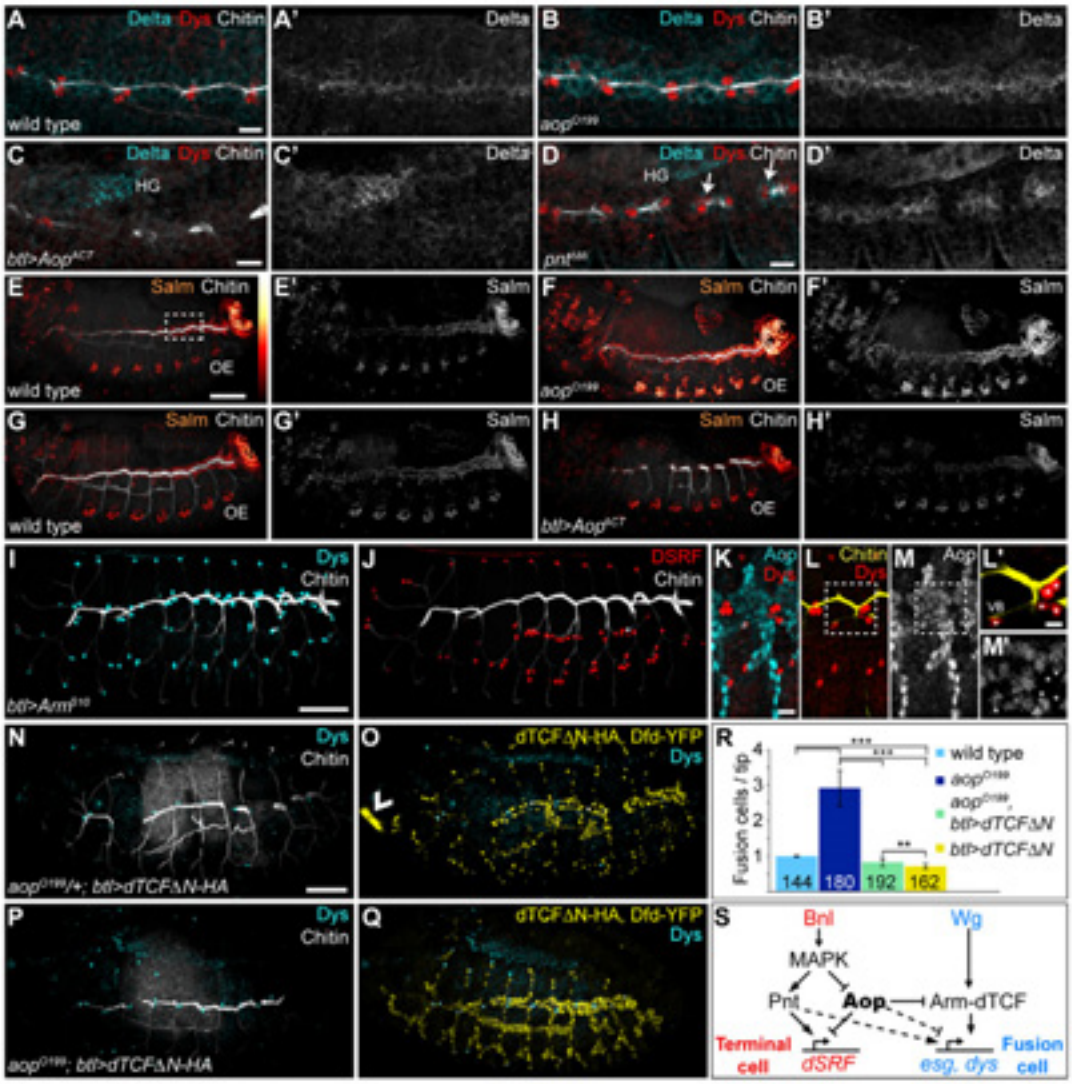

Fig. 4. Aop blocks fusion cell specification in the dorsal trunk by antagonizing Wingless signaling. (**A**,**A′**) In wild-type embryos, the Wingless target Delta (A′, cyan in A) is expressed at higher levels in DT FCs (red in A) compared with the rest of DT cells at stage 13. (**B**,**B′**) In *aop*^{O199} embryos, Delta levels are elevated in most DT cells. (**C**,**C′**) Conversely, Delta levels are dramatically reduced in embryos expressing Aop^{ACT} in tracheal cells. (**D**,**D′**) By contrast, Delta levels in *pnt*$^{\Delta 88}$ embryos are comparable with those in wild-type embryos. Supernumerary FCs are present (red in D; arrows indicate supernumerary cells) in the DT of the *pnt*$^{\Delta 88}$ embryo. Delta expression in non-tracheal cells (hindgut; HG) cells is indicated in C,D. (**E-H′**) Salm is expressed in a Wg-dependent manner in tracheal DT cells. Salm signal intensities are color-coded using a heat map (E; black=0, white=255). Salm levels were quantified in DT Tr8-9 (box in E). *aop*^{O199} embryos (F) show elevated (1.2±0.3 fold, P<0.001) Salm levels compared with wild-type control embryos from the same staining (E). Conversely, embryos expressing Aop^{ACT} (H) in tracheal cells show lower (0.7±0.1 fold, P<0.001) Salm levels compared with wild-type controls from the same staining (G). Salm levels in oenocytes (OE) are comparable between wild-type and *btl* >Aop^{ACT} embryos (E,G,H), whereas Salm levels are increased in *aop* loss-of-function embryos (F). (**I**,**J**) Tracheal expression of constitutively active Arm (Arm^{S10}) causes specification of supernumerary FCs (cyan in I) in DT, VB and transverse connective branches. The number of TCs (red in J) is normal in most branches and only slightly reduced in the VB. (**K-M′**) Aop (M, cyan in K) is absent from supernumerary FCs (red in K,L) in Arm^{S10}-expressing embryos. L′ and M′ show enlargements of the boxed regions in L,M. Asterisks indicate FC nuclei. VB, visceral branch. (**N-Q**) Tracheal expression of dominant-negative dTCF (dTCFΔN-HA, yellow in O,Q) in *aop*^{O199}/+ (N,O) heterozygous embryos causes reduced DT fusion cell number and DT breaks. Expression of dTCFΔN-HA in *aop*^{O199} homozygotes suppresses supernumerary DT fusion cell formation (P; compare with Fig. 2I). Embryos were genotyped using dTCFΔN-HA and Dfd-YFP (arrowhead in O) staining. (**R**) Quantification of DT fusion cells. Genotypes are indicated. dTCFΔN-HA expression suppresses supernumerary FC formation in *aop*^{O199} mutants. Numbers inside bars indicate numbers of branch tips scored for each genotype. Error bars represent s.d. ***P≤0.001; **P≤0.01. (**S**) Proposed model of dual role of Aop in TC and FC specification. Scale bars: 10 µm in A-D′,K-M′; 50 µm in E-H′,I,J,N-Q.

mutants, dTCFΔN suppressed FC specification to nearly the same level as it did in a wild-type background (Fig. 4P-R). Importantly, however, dTCFΔN expression did not affect DT tube morphology, suggesting that DT identity was largely unimpaired by the partially reduced Wg signal in this situation (Fig. 4N,P). These results show that FC mis-specification upon loss of *aop* requires TCF function, consistent with the idea that *aop* antagonizes Wg signaling at the level of Arm (Olson et al., 2011). Interestingly, although tracheal expression of Delta and Dys was lost in Aop^{ACT}-expressing embryos (Fig. 4C), their expression was maintained in *pnt* mutants (Fig. 4D), suggesting that Aop regulates Wg target gene expression through a mechanism that is independent of *pnt* function. As Wg

signaling in the tracheae is confined to the DT region (Llimargas, 2000), *aop*-dependent inhibition of Wg signaling explains why supernumerary FCs in *aop* mutants are restricted to the DT. In addition, Aop blocks MAPK signaling in non-tip cells of the other tracheal branches and thereby prevents these cells from adopting TC fate. Thus, *aop* plays a dual role in controlling FC and TC specification by inhibiting Wg and MAPK signaling (Fig. 4S).

The choice between fusion and terminal cell fate is constrained by the selector gene *salm*

Our results show that most or all tracheal cells are competent to adopt a specialized fate if the Aop inhibitory block is absent. However, the chosen fate (FC or TC) depends on the position of the cell in the tracheal system. Region-specific cell fate choice results in part from the distinct distribution of signals (Wg, Bnl) that act on cells in different regions of the tracheal primordium. We hypothesized that branch-specific selector genes could constrain the competence of tracheal cells to adopt a given fate in response to the inductive signals. Consistent with this scenario, global misexpression of *bnl* causes most tracheal cells to acquire TC fate (Sutherland et al., 1996; Gervais and Casanova, 2011), whereas DT cells are mainly mis-specified as FCs (supplementary material Fig. S3). Importantly, global Bnl misexpression causes degradation of Aop (Ohshiro et al., 2002) and MAPK phosphorylation (Gervais and Casanova, 2011) in all tracheal cells, suggesting that all tracheal cells are equally competent to receive the Bnl signal, but that the downstream responses are branch specific. One branch identity gene with key roles in subdividing the tracheal primordium is the selector gene *salm* (Kühnlein and Schuh, 1996). Tracheal *salm* expression becomes restricted to the DT, where it is sustained by Wg signaling and determines DT identity (Fig. 4E) (Kühnlein and Schuh, 1996; Llimargas, 2000; Franch-Marro and Casanova, 2002). In *salm* mutants, cells of the DT region migrate dorsoventrally instead of anteroposteriorly and assume VB identity (Fig. 5A,B; chitin staining showing branch architecture) (Franch-Marro and Casanova, 2002). Conversely, pan-tracheal *salm* misexpression transforms most branches into multicellular DT-like tubes (Fig. 5E,F) (Ribeiro et al., 2004). To determine whether *salm* influences the choice between the two tip cell fates, we analyzed FC and TC induction in *salm* mutants and in *salm* misexpressing embryos. In both situations, only tip cells differentiated into FCs or TCs, but the choice between the two fates reflected the transformed identity of each branch. In *salm* mutants, where dorsal tracheal cells were transformed into ventral identity, the tips of the transformed branches contained TCs and FCs, as in the lateral trunk of wild-type embryos (Fig. 5A,B) (Franch-Marro and Casanova, 2002). Conversely, upon *salm* misexpression, VB cells were transformed into DT identity and the tip cells assumed FC fate (Fig. 5E,F, arrows). We also noticed that in this situation overall TC number was dramatically reduced. The altered tip cell fate choice becomes more evident when the *aop*-mediated differentiation block is released: in *aop salm* double mutants, FC specification was not changed compared with $salm^{1}$ mutants (Fig. 5C,D). Interestingly, however, the transformed DT cells now became TCs, the default fate of the VB tip cells, instead of FCs. Conversely, misexpression of *salm* in aop^{O199} mutants led to supernumerary FC formation throughout the tracheae, whereas TC formation was largely suppressed (Fig. 5G,H). Thus, *salm* is necessary and sufficient to constrain the competence of tracheal cells towards FC fate.

As Wg signaling is required to maintain tracheal *salm* expression, it is formally possible that Wg acts solely via *salm* to control FC induction. In this scenario, ectopic *salm* expression should obviate the requirement for Wg in FC induction. To test this idea, we blocked Wg signaling by overexpressing Axin-GFP in tracheal cells, and then asked whether co-overexpression of *salm* is sufficient to rescue FC specification in the absence of Wg signaling (Fig. 6A-C). As expected, Axin-GFP expression nearly completely abolished FC induction and DT formation (Fig. 6A) (Chihara and Hayashi, 2000). Co-expression of Arm^{S10} restored both FC induction and DT formation (Fig. 6B). By contrast, co-expressing *salm* with Axin-GFP failed to restore FC formation, although *salm* overexpression was sufficient to transform the remaining tracheal branches towards DT identity, as indicated by their characteristic lumen morphology (Fig. 6C). Consistent with these results, Delta expression was upregulated more strongly by constitutively activating Wg signaling (through Arm^{S10} expression; Fig. 6G-I) than by overexpressing *salm* (Fig. 6J-L) when compared with wild-type embryos (Fig. 6D-F). Furthermore, *salm* expression was previously shown to restore DT identity, but not DT fusion defects in *arm* mutants (Llimargas, 2000). These results indicate that *salm* expression is not sufficient for FC induction and suggest that other Wg targets besides *salm* are required to induce FCs in the DT. Thus, expression of the selector gene *salm* is not only necessary to specify branch identity but also to constrain the choice between alternative tip cell types in response to MAPK signaling.

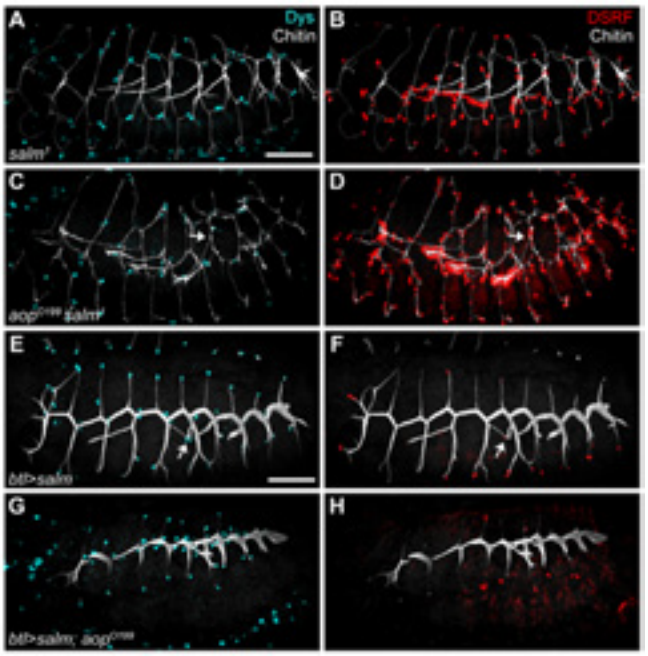

Fig. 5. The selector gene *salm* constrains the choice between fusion cell and terminal cell fate. (A-H) Stage 15 embryos stained for tracheal lumen (chitin; white), FCs (Dys; cyan) and TCs (DSRF; red). (**A**,**B**) In $salm^{1}$ mutants, DT cells are transformed and migrate dorsoventrally instead of anteroposteriorly. The pattern of tip cell specification reflects the branch transformation. (**C**,**D**) In aop^{O199} $salm^{1}$ double mutant embryos, most cells, including the transformed DT cells (arrows), differentiate into TCs. (**E**,**F**) Misexpression of *salm* throughout the tracheal system largely abolishes formation of TCs (F), but not FCs (E). Some VB tip cells (arrows) acquire FC fate instead of TC fate, consistent with a transformation of VB towards DT branch identity. (**G**,**H**) Misexpression of *salm* in aop^{O199} mutants leads to supernumerary FC formation throughout the tracheal system, whereas TC formation is largely suppressed. Scale bars: 50 μm.

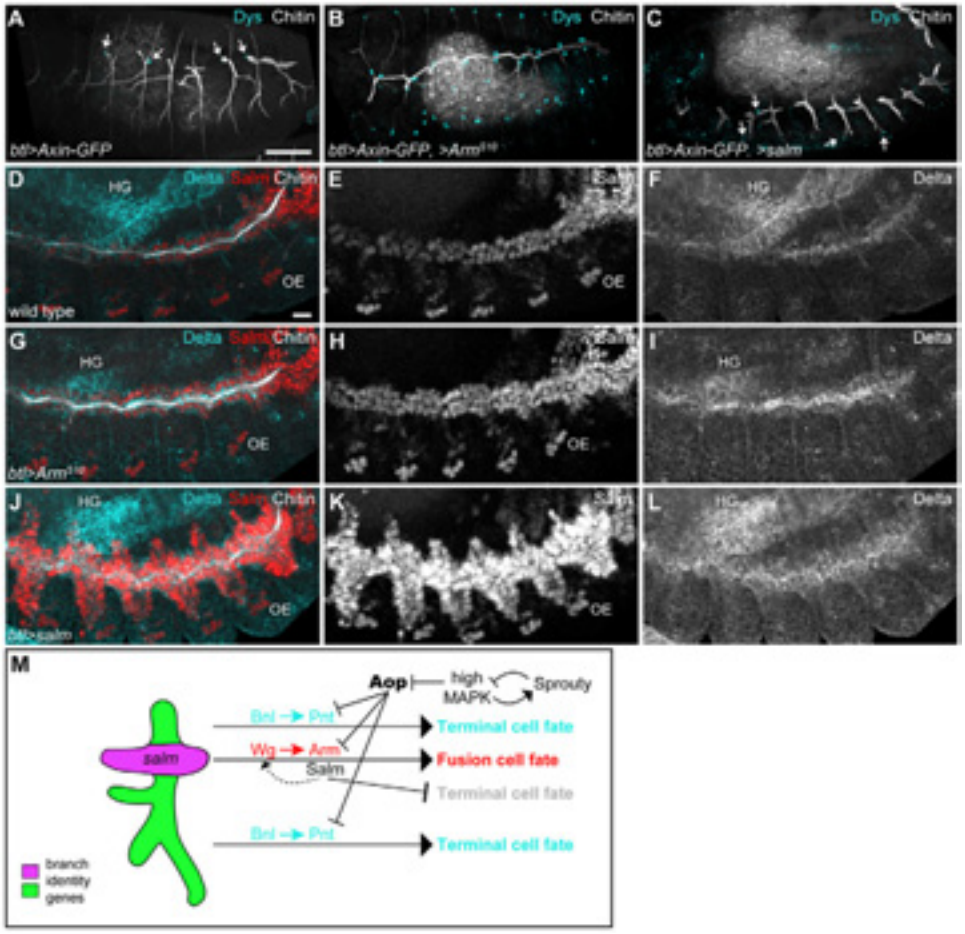

Fig. 6. Salm expression is not sufficient to trigger fusion cell specification. (**A-C**) Expression of Axin-GFP in tracheal cells abolishes DT formation and FC specification (A; remaining FCs are indicated by arrows). Arm^{S10} expression in this background restores DT formation and FC specification (B). By contrast, *salm* expression fails to restore FC specification and DT fusion, although it is sufficient to transform tracheal branches towards DT identity, as indicated by the large diameter of chitin-labeled tracheal lumen (C). FCs are indicated by arrows in C. In A, UAS-Axin-GFP is co-expressed with UAS-mCherry-NLS (not shown) to maintain copy number of UAS sites equal between genotypes in A-C. (**D-L**) Immunostaining of Salm and Delta in stage 14 wild-type (D-F), Arm^{S10}-expressing (G-I) and *salm*-overexpressing (J-L) embryos. Expression of Arm^{S10} in tracheal cells leads to a moderate increase of tracheal Salm (H, red in G) levels, whereas tracheal Delta levels (I, cyan in G) are more strongly increased. Embryos overexpressing *salm* show higher Salm levels (K, red in J) in tracheal cells compared with wild-type and Arm^{S10}-expressing embryos, but only slightly increased Delta levels (L, cyan in J) compared with wild-type control embryos. Non-tracheal expression of Salm in oenocytes (OE) and of Delta in the Hindgut (HG) is indicated. Salm levels in oenocytes (OE) remain similar between genotypes. (**M**) Model of tip cell specification. The combination of inductive signals (Bnl, Wg) and branch identity gene (*salm*, *knirps*) expression determines tip cell fate in a branch-specific manner. Aop antagonizes both MAPK and Wg signaling, and restricts differentiation to branch tips, where MAPK signaling triggers Aop degradation. Scale bars: 50 μm in A-C; 10 μm in D-L.

DISCUSSION

In this work we have investigated how the choice between the two types of specialized tip cells in the tracheal system is controlled. We show that the transcriptional repressor Aop plays a key role in linking tracheal tip cell fate selection with branch identity. First, we describe a novel tube morphogenesis phenotype in *aop* mutants, which is due to the massive mis-specification of regular epithelial cells into specialized tracheal tip cells. We show that *aop* is specifically required for controlling tracheal cell fate, whereas *aop*, like *pnt* (Samakovlis et al., 1996a; Ribeiro et al., 2002), is dispensable for primary tracheal branching, thus uncoupling roles of RTK signaling in cell fate specification and cell motility. Our finding that tracheal branching morphogenesis proceeds normally in the presence of excess tip cell-like cells suggests that collective cell migration is surprisingly robust and that mis-specified cells apparently do not impede the guided migration of the tracheal primordium. Second, we demonstrate that in the absence of inhibitors of MAPK signaling (*aop* and *sty*), all tracheal cells are competent to assume either TC or FC fate. The transcriptional repressor Aop globally blocks both TC and FC differentiation, but high-levels of MAPK signaling in tip cells relieve Aop-mediated inhibition, thus permitting differentiation. Third, our results suggest that in the DT region Aop limits FC induction through a distinct mechanism by antagonizing Wg signaling in addition to MAPK signaling. Conversely, in the other branches, Aop limits TC differentiation by blocking MAPK-dependent activation of Pnt (Hacohen et al., 1998). Fourth, we show that the region-specific choice between the two cell fates in the DT is determined by Wg signaling and by the selector gene *salm*. Based on these results, we propose a model in which a single repressor, Aop, integrates MAPK and Wg signals to couple tip cell fate selection with branch identity (Fig. 6M). High levels of Bnl signaling trigger Pnt activation and

Aop degradation in tracheal tip cells. We propose that in the DT, unlike in other tracheal cells, MAPK-induced degradation of Aop releases inhibition of Wg signaling. This is consistent with recent work showing an inhibitory effect of Aop on Wg signaling, possibly through direct interaction of Aop and Arm (Olson et al., 2011), or through Aop-mediated transcriptional repression of Wg pathway components (Webber et al., 2012). Our work extends the evidence for this unexpected intersection between two major conserved signaling pathways, suggesting that this function of Aop is likely to be more widespread than previously appreciated. Our findings also provide an explanation for the puzzling observation that, in *pnt* mutants, TCs are lost, while FCs become ectopically specified (Samakovlis et al., 1996a). As *pnt* is required for expression of the feedback inhibitor *sty* (Hacohen et al., 1998), loss of *pnt* is expected to lead to MAPK pathway activation and consequently to increased Aop degradation. This would release Aop-mediated repression of Wg signaling, resulting in extra FCs, whereas TCs are absent because of the lack of *pnt*-dependent induction. This suggests that excessive FC specification in the DT of *aop* and *sty* mutants is mainly due to deregulated Wg signaling, rather than to de-repression of *pnt*-dependent MAPK target genes. Consistent with this notion, we showed that *pnt* is not required for Delta and Dys expression in tracheal cells, although constitutively active Aop^{ACT} represses their expression.

Our results further show that *salm* function constrains the fate that is chosen by cells when released from the Aop inhibitory block. MAPK signaling triggers Aop degradation in all tip cells, but only in the absence of *salm* does this signal lead to TC induction. In *salm*-expressing cells, degradation of Aop releases Wg signaling, resulting in FC specification. Thus, *salm* biases the choice between two morphologically different types of seamless tubes. This is reminiscent of the role of *salm* in switching between different cell types in the peripheral nervous system and in muscles (Elstob et al., 2001; Rusten et al., 2001; Schönbauer et al., 2011). We show that *salm* expression is sufficient to repress TC formation. Our genetic results, consistent with biochemical data showing that Salm acts as a transcriptional repressor (Sánchez et al., 2011), suggest that *salm* promotes FC fate by repressing genes involved in TC development. However, *salm* is not sufficient to overcome the requirement for Wg signaling in FC induction, indicating that Wg does not act solely via *salm* to induce FC fate. Indeed, FC induction requires genes whose expression is independent of *salm* (*esg*, *dys*) (Chihara and Hayashi, 2000; Jiang et al., 2010). In addition, we propose that a feedback loop between Wg signaling and *salm* expression maintains levels of Wg signaling in the DT sufficiently high to induce FC fate (Fig. 6M). Taken together, these results suggest that the default specialized tip cell fate, and possibly an ancestral tracheal cell state, is TC fate. Although FCs and TCs differ in their morphology, they share a unique topology as seamless unicellular tubes (Uv et al., 2003). FCs and TCs might therefore represent variations of a prototypical seamless tube cell type. Salm might modify cellular morphology by repressing TC genes, including *DSRF*, which mediates cell elongation and shape change (Gervais and Casanova, 2011). Intriguingly, Wg-dependent *salm* expression in the DT of dipterans correlates with a shift towards FC as the specialized fate adopted by the tip cells of this branch (X. Franch-Marro, personal communication). We showed that *salm* expression inhibits TC fate, while promoting the formation of a multicellular main tracheal tube by inhibiting cell intercalation (Ribeiro et al., 2004). It is therefore tempting to speculate that the *salm*-dependent switch from a branching towards an anastomosing tip cell type in the DT may have evolved with the acquisition in higher insects of a main tube that connects separate tracheal primordia to generate a tubular network. It will be of great interest to identify the relevant target genes that mediate the effect of Salm on tube morphology and tip cell fate.

The mechanisms of tip cell selection during angiogenesis in vertebrates are beginning to be understood at the molecular level (Ellertsdóttir et al., 2010; Geudens and Gerhardt, 2011; Herbert and Stainier, 2011). However, the signals that control the formation of vascular anastomoses by a particular set of tip cells are not known. Intriguingly, the development of secondary lumina in *aop* mutants is reminiscent of transluminal pillar formation during intussusceptive angiogenesis, which is thought to subdivide an existing vessel without sprouting (Burri et al., 2004). Although the cellular basis for this process is not understood, it is conceivable that specialized endothelial cells are involved in transluminal pillar formation. Our work provides a paradigm for deciphering how two major signaling pathways crosstalk and are integrated to control cell fate in a developing tubular organ. It will be interesting to see whether similar principles govern tip cell fate choice during tube morphogenesis in vertebrates and invertebrates.

Acknowledgements
Kristina Armbruster isolated the aop^{O199} mutant. We thank Markus Affolter, Konrad Basler, Yang Hong, Lan Jiang, Christian Klämbt, Mark Krasnow, Reinhard Schuh, Robert Ward, Yinhua Zhang (New England Biolabs), the Bloomington *Drosophila* Stock Center, and the Developmental Studies Hybridoma Bank for providing fly stocks and reagents. We thank Markus Affolter, Jordi Casanova, Dominique Förster, Xavier Franch-Marro and Shigeo Hayashi for discussions and comments on the manuscript, and Jordi Casanova and Xavier Franch-Marro for helpful discussions on the evolution of tracheal systems. We are indebted to Christian Lehner for continuous support and discussions.

Funding
This work was supported by the Swiss National Science Foundation [SNF 31003A_141093_1], the Julius Klaus-Stiftung Zürich, the University of Zürich and the Kanton Zürich. S.C. is supported by a Forschungskredit fellowship of the University of Zürich.

Competing interests statement
The authors declare no competing financial interests.

Supplementary material
Supplementary material available online at
http://dev.biologists.org/lookup/suppl/doi:10.1242/dev.087874/-/DC1

References
Affolter, M. and Caussinus, E. (2008). Tracheal branching morphogenesis in Drosophila: new insights into cell behaviour and organ architecture. *Development* **135**, 2055-2064.
Brunner, D., Dücker, K., Oellers, N., Hafen, E., Scholz, H. and Klämbt, C. (1994). The ETS domain protein pointed-P2 is a target of MAP kinase in the sevenless signal transduction pathway. *Nature* **370**, 386-389.
Burri, P. H., Hlushchuk, R. and Djonov, V. (2004). Intussusceptive angiogenesis: its emergence, its characteristics, and its significance. *Dev. Dyn.* **231**, 474-488.
Chihara, T. and Hayashi, S. (2000). Control of tracheal tubulogenesis by Wingless signaling. *Development* **127**, 4433-4442.
Cliffe, A., Hamada, F. and Bienz, M. (2003). A role of Dishevelled in relocating Axin to the plasma membrane during wingless signaling. *Curr. Biol.* **13**, 960-966.
Dossenbach, C., Röck, S. and Affolter, M. (2001). Specificity of FGF signaling in cell migration in Drosophila. *Development* **128**, 4563-4572.
Ellertsdóttir, E., Lenard, A., Blum, Y., Krudewig, A., Herwig, L., Affolter, M. and Belting, H. G. (2010). Vascular morphogenesis in the zebrafish embryo. *Dev. Biol.* **341**, 56-65.
Elstob, P. R., Brodu, V. and Gould, A. P. (2001). spalt-dependent switching between two cell fates that are induced by the Drosophila EGF receptor. *Development* **128**, 723-732.
Förster, D., Armbruster, K. and Luschnig, S. (2010). Sec24-dependent secretion drives cell-autonomous expansion of tracheal tubes in Drosophila. *Curr. Biol.* **20**, 62-68.
Franch-Marro, X. and Casanova, J. (2002). spalt-induced specification of distinct dorsal and ventral domains is required for Drosophila tracheal patterning. *Dev. Biol.* **250**, 374-382.

Gervais, L. and Casanova, J. (2011). The Drosophila homologue of SRF acts as a boosting mechanism to sustain FGF-induced terminal branching in the tracheal system. *Development* **138**, 1269-1274.
Geudens, I. and Gerhardt, H. (2011). Coordinating cell behaviour during blood vessel formation. *Development* **138**, 4569-4583.
Ghabrial, A., Luschnig, S., Metzstein, M. M. and Krasnow, M. A. (2003). Branching morphogenesis of the Drosophila tracheal system. *Annu. Rev. Cell Dev. Biol.* **19**, 623-647.
Guillemin, K., Groppe, J., Ducker, K., Treisman, R., Hafen, E., Affolter, M. and Krasnow, M. A. (1996). The pruned gene encodes the Drosophila serum response factor and regulates cytoplasmic outgrowth during terminal branching of the tracheal system. *Development* **122**, 1353-1362.
Hacohen, N., Kramer, S., Sutherland, D., Hiromi, Y. and Krasnow, M. A. (1998). sprouty encodes a novel antagonist of FGF signaling that patterns apical branching of the Drosophila airways. *Cell* **92**, 253-263.
Herbert, S. P. and Stainier, D. Y. (2011). Molecular control of endothelial cell behaviour during blood vessel morphogenesis. *Nat. Rev. Mol. Cell Biol.* **12**, 551-564.
Herwig, L., Blum, Y., Krudewig, A., Ellertsdottir, E., Lenard, A., Belting, H. G. and Affolter, M. (2011). Distinct cellular mechanisms of blood vessel fusion in the zebrafish embryo. *Curr. Biol.* **21**, 1942-1948.
Huang, J., Zhou, W., Dong, W., Watson, A. M. and Hong, Y. (2009). From the Cover: Directed, efficient, and versatile modifications of the Drosophila genome by genomic engineering. *Proc. Natl. Acad. Sci. USA* **106**, 8284-8289.
Ikeya, T. and Hayashi, S. (1999). Interplay of Notch and FGF signaling restricts cell fate and MAPK activation in the Drosophila trachea. *Development* **126**, 4455-4463.
Jiang, L. and Crews, S. T. (2003). The Drosophila dysfusion basic helix-loop-helix (bHLH)-PAS gene controls tracheal fusion and levels of the trachealess bHLH-PAS protein. *Mol. Cell. Biol.* **23**, 5625-5637.
Jiang, L., Pearson, J. C. and Crews, S. T. (2010). Diverse modes of Drosophila tracheal fusion cell transcriptional regulation. *Mech. Dev.* **127**, 265-280.
Kramer, S., Okabe, M., Hacohen, N., Krasnow, M. A. and Hiromi, Y. (1999). Sprouty: a common antagonist of FGF and EGF signaling pathways in Drosophila. *Development* **126**, 2515-2525.
Kühnlein, R. P. and Schuh, R. (1996). Dual function of the region-specific homeotic gene spalt during Drosophila tracheal system development. *Development* **122**, 2215-2223.
Lai, Z. C. and Rubin, G. M. (1992). Negative control of photoreceptor development in Drosophila by the product of the yan gene, an ETS domain protein. *Cell* **70**, 609-620.
Le, T., Liang, Z., Patel, H., Yu, M. H., Sivasubramaniam, G., Slovitt, M., Tanentzapf, G., Mohanty, N., Paul, S. M., Wu, V. M. et al. (2006). A new family of Drosophila balancer chromosomes with a w- dfd-GMR yellow fluorescent protein marker. *Genetics* **174**, 2255-2257.
Lee, T., Hacohen, N., Krasnow, M. and Montell, D. J. (1996). Regulated Breathless receptor tyrosine kinase activity required to pattern cell migration and branching in the Drosophila tracheal system. *Genes Dev.* **10**, 2912-2921.
Llimargas, M. (1999). The Notch pathway helps to pattern the tips of the Drosophila tracheal branches by selecting cell fates. *Development* **126**, 2355-2364.
Llimargas, M. (2000). Wingless and its signalling pathway have common and separable functions during tracheal development. *Development* **127**, 4407-4417.
Maruyama, R. and Andrew, D. J. (2012). Drosophila as a model for epithelial tube formation. *Dev. Dyn.* **241**, 119-135.
Montagne, J., Groppe, J., Guillemin, K., Krasnow, M. A., Gehring, W. J. and Affolter, M. (1996). The Drosophila Serum Response Factor gene is required for the formation of intervein tissue of the wing and is allelic to blistered. *Development* **122**, 2589-2597.
Nusslein-Volhard, C., Wieschaus, E. and Kluding, H. (1984). Mutations affecting the pattern of the larval cuticle in Drosophila melanogaster. I. Zygotic loci on the second chromosome. *Roux's Arch. Dev. Biol.* **193**, 267-282.
Ohshiro, T., Emori, Y. and Saigo, K. (2002). Ligand-dependent activation of breathless FGF receptor gene in Drosophila developing trachea. *Mech. Dev.* **114**, 3-11.
Olson, E. R., Pancratov, R., Chatterjee, S. S., Changkakoty, B., Pervaiz, Z. and DasGupta, R. (2011). Yan, an ETS-domain transcription factor, negatively modulates the Wingless pathway in the Drosophila eye. *EMBO Rep.* **12**, 1047-1054.
Pai, L. M., Orsulic, S., Bejsovec, A. and Peifer, M. (1997). Negative regulation of Armadillo, a Wingless effector in Drosophila. *Development* **124**, 2255-2266.
Queenan, A. M., Ghabrial, A. and Schüpbach, T. (1997). Ectopic activation of torpedo/Egfr, a Drosophila receptor tyrosine kinase, dorsalizes both the eggshell and the embryo. *Development* **124**, 3871-3880.
Rebay, I. (2002). Keeping the receptor tyrosine kinase signaling pathway in check: lessons from Drosophila. *Dev. Biol.* **251**, 1-17.
Rebay, I. and Rubin, G. M. (1995). Yan functions as a general inhibitor of differentiation and is negatively regulated by activation of the Ras1/MAPK pathway. *Cell* **81**, 857-866.
Ribeiro, C., Ebner, A. and Affolter, M. (2002). In vivo imaging reveals different cellular functions for FGF and Dpp signaling in tracheal branching morphogenesis. *Dev. Cell* **2**, 677-683.
Ribeiro, C., Neumann, M. and Affolter, M. (2004). Genetic control of cell intercalation during tracheal morphogenesis in Drosophila. *Curr. Biol.* **14**, 2197-2207.
Rogge, R., Green, P. J., Urano, J., Horn-Saban, S., Mlodzik, M., Shilo, B. Z., Hartenstein, V. and Banerjee, U. (1995). The role of yan in mediating the choice between cell division and differentiation. *Development* **121**, 3947-3958.
Rusten, T. E., Cantera, R., Urban, J., Technau, G., Kafatos, F. C. and Barrio, R. (2001). Spalt modifies EGFR-mediated induction of chordotonal precursors in the embryonic PNS of Drosophila promoting the development of oenocytes. *Development* **128**, 711-722.
Samakovlis, C., Hacohen, N., Manning, G., Sutherland, D. C., Guillemin, K. and Krasnow, M. A. (1996a). Development of the Drosophila tracheal system occurs by a series of morphologically distinct but genetically coupled branching events. *Development* **122**, 1395-1407.
Samakovlis, C., Manning, G., Steneberg, P., Hacohen, N., Cantera, R. and Krasnow, M. A. (1996b). Genetic control of epithelial tube fusion during Drosophila tracheal development. *Development* **122**, 3531-3536.
Sánchez, J., Talamillo, A., González, M., Sánchez-Pulido, L., Jiménez, S., Pirone, L., Sutherland, J. D. and Barrio, R. (2011). Drosophila Sal and Salr are transcriptional repressors. *Biochem. J.* **438**, 437-445.
Schönbauer, C., Distler, J., Jährling, N., Radolf, M., Dodt, H. U., Frasch, M. and Schnorrer, F. (2011). Spalt mediates an evolutionarily conserved switch to fibrillar muscle fate in insects. *Nature* **479**, 406-409.
Shiga, Y., Tanaka-Matakatsu, M. and Hayashi, S. (1996). A nuclear GFP/ beta-galactosidase fusion protein as a marker for morphogenesis in living Drosophila. *Dev. Growth Differ.* **38**, 99-106.
Steneberg, P., Hemphälä, J. and Samakovlis, C. (1999). Dpp and Notch specify the fusion cell fate in the dorsal branches of the Drosophila trachea. *Mech. Dev.* **87**, 153-163.
Sutherland, D., Samakovlis, C. and Krasnow, M. A. (1996). branchless encodes a Drosophila FGF homolog that controls tracheal cell migration and the pattern of branching. *Cell* **87**, 1091-1101.
Tanaka-Matakatsu, M., Uemura, T., Oda, H., Takeichi, M. and Hayashi, S. (1996). Cadherin-mediated cell adhesion and cell motility in Drosophila trachea regulated by the transcription factor Escargot. *Development* **122**, 3697-3705.
Tei, H., Nihonmatsu, I., Yokokura, T., Ueda, R., Sano, Y., Okuda, T., Sato, K., Hirata, K., Fujita, S. C. and Yamamoto, D. (1992). pokkuri, a Drosophila gene encoding an E-26-specific (Ets) domain protein, prevents overproduction of the R7 photoreceptor. *Proc. Natl. Acad. Sci. USA* **89**, 6856-6860.
Uv, A., Cantera, R. and Samakovlis, C. (2003). Drosophila tracheal morphogenesis: intricate cellular solutions to basic plumbing problems. *Trends Cell Biol.* **13**, 301-309.
van de Wetering, M., Cavallo, R., Dooijes, D., van Beest, M., van Es, J., Loureiro, J., Ypma, A., Hursh, D., Jones, T., Bejsovec, A. et al. (1997). Armadillo coactivates transcription driven by the product of the Drosophila segment polarity gene dTCF. *Cell* **88**, 789-799.
Wappner, P., Gabay, L. and Shilo, B. Z. (1997). Interactions between the EGF receptor and DPP pathways establish distinct cell fates in the tracheal placodes. *Development* **124**, 4707-4716.
Watanabe, T., Ito, Y., Yamada, T., Hashimoto, M., Sekine, S. and Tanaka, H. (1994). The roles of the C-terminal domain and type III domains of chitinase A1 from Bacillus circulans WL-12 in chitin degradation. *J. Bacteriol.* **176**, 4465-4472.
Webber, J. L., Zhang, J., Cote, L., Vivekanand, P., Ni, X., Zhou, J., Nègre, N., Carthew, R. W., White, K. P. and Rebay, I. (2012). The relationship between long-range chromatin occupancy and polymerization of the Drosophila ETS family transcriptional repressor Yan. *Genetics* doi: 10.1534/genetics.112.146647.
Zhang, L. and Ward, R. E., 4th (2009). uninflatable encodes a novel ectodermal apical surface protein required for tracheal inflation in Drosophila. *Dev. Biol.* **336**, 201-212.

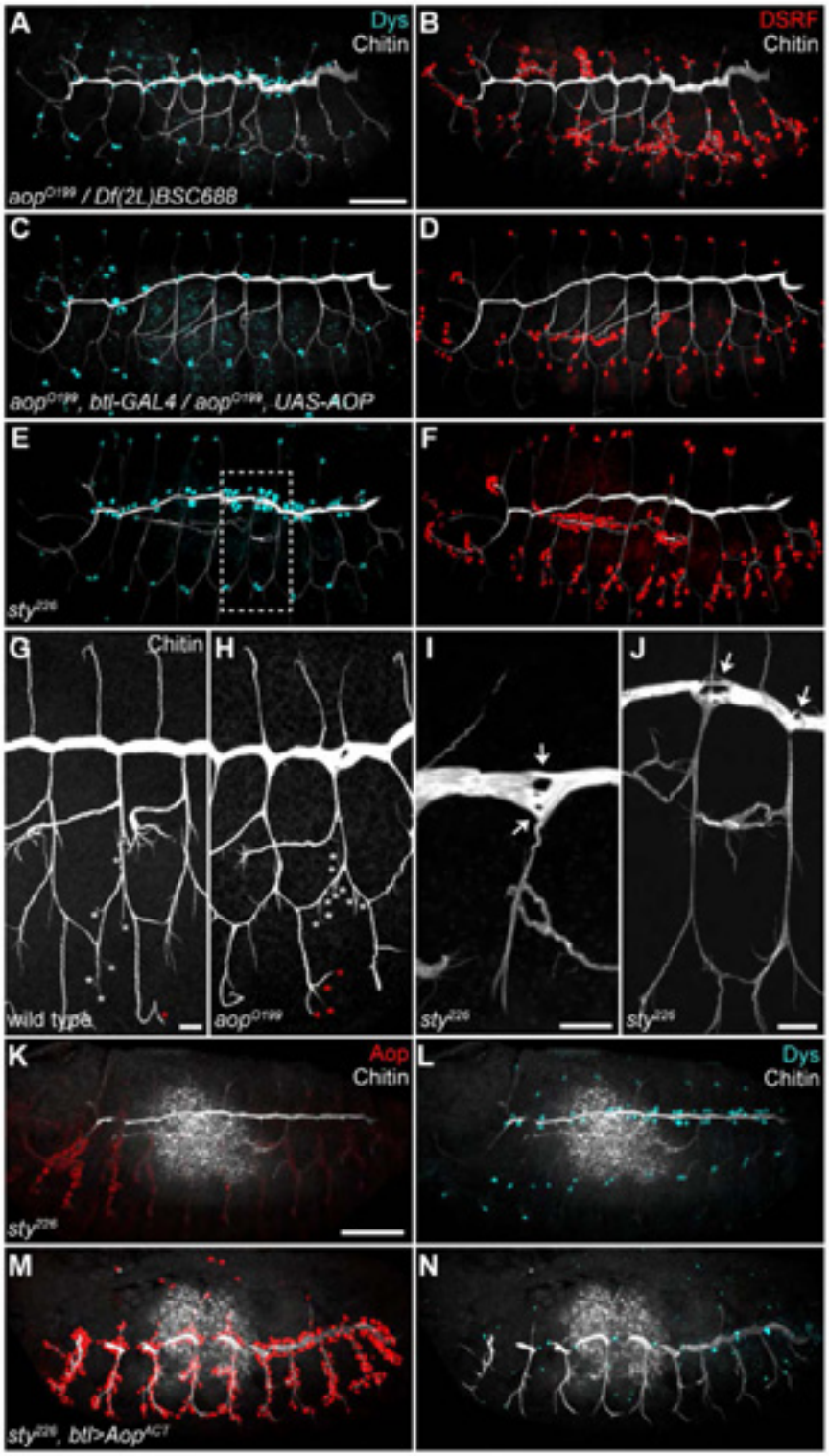

Fig. S1. *sty* mutants show similar mis-specification of fusion cells and terminal cells as *aop* mutants. (**A**,**B**) Stage 15-16 embryos stained for chitin (white), Dys (cyan, FCs) and DSRF (red, TCs). Hemizygous aop^{O199}/Df(2L)BSC688 embryos show defects resembling those of aop^{O199} homozygous embryos (see Fig. 2), indicating that aop^{O199} is an amorphic allele. (**C**,**D**) Tracheal-specific expression of *aop* under the control of *btl-GAL4* completely rescues the tracheal defects of aop^{O199} embryos, but does not rescue embryonic lethality and the head involution defect of aop^{O199} embryos (data not shown). Rescued embryos show normal numbers of FCs and TCs. (**E**,**F**) sty^{226} embryos show supernumerary FCs in the DT (E) and extra TCs in the remaining branches (F). (**G**,**H**) Higher magnifications of wild-type (G) and aop^{O199} (H) embryos stained for chitin show fine terminal branches in the lateral trunk (white asterisks) and in the ganglionic branch (red asterisks). Additional terminal branches are present in the aop^{O199} embryo. (I,J) Higher magnifications of the DT in sty^{226} embryos stained for chitin. The bifurcations in the DT lumen (arrows) resemble the *aop* phenotype (J is an enlargement of the area outlined in E). (K-N) Expression of Aop^{ACT} (detected by Aop antibody, red in M) in sty^{226} mutants suppresses ectopic FC specification in the DT in the absence of *sty* function (compare N with L). Scale bars: 50 μm in A-F,K-N; 10 μm in G-J.

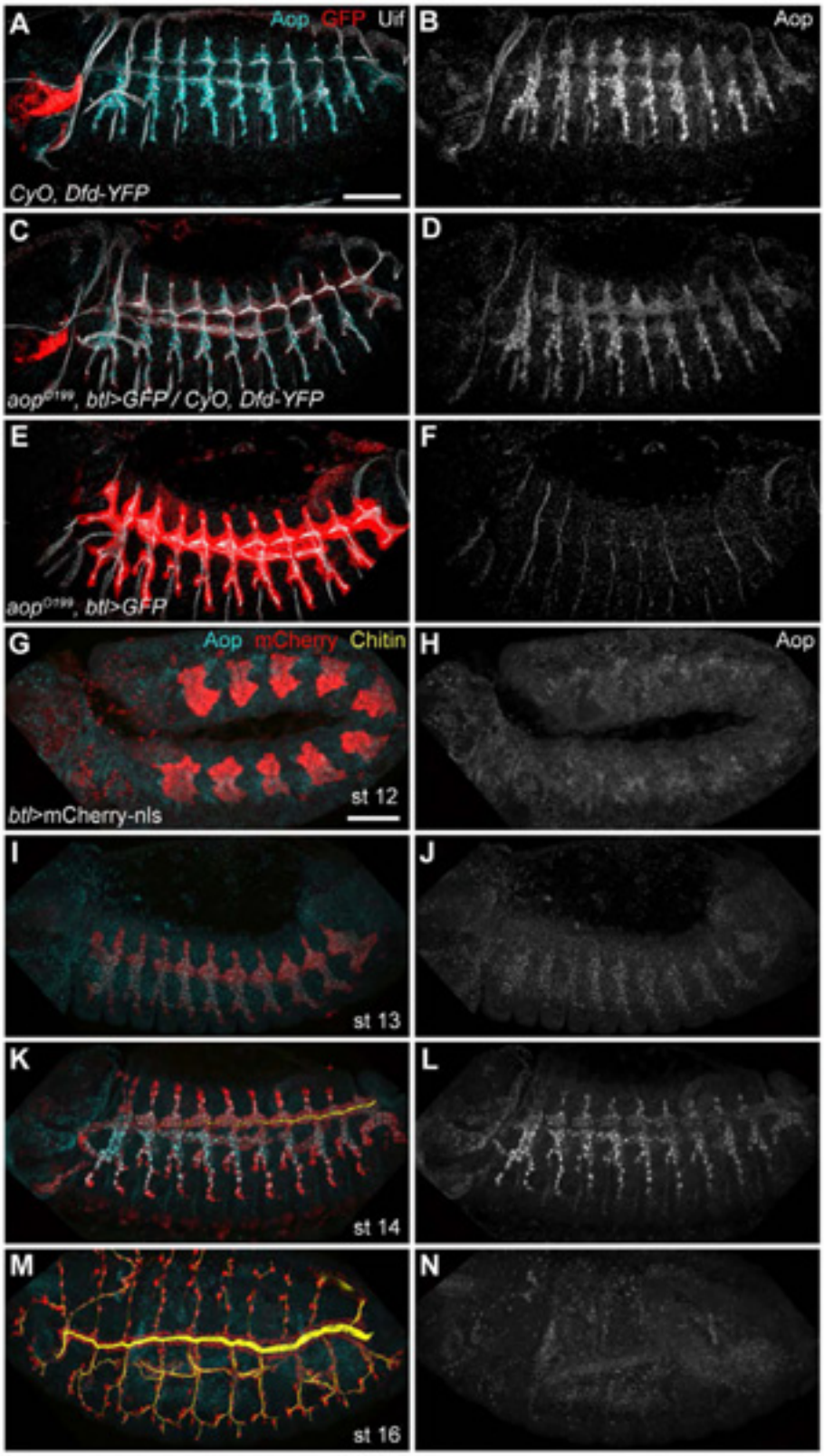

Fig. S2. Aop expression during tracheal development. (**A-F**) Stage 13 embryos from the parental genotype *aop^{O199} btl-Gal4 UAS-GFP UAS-Verm-mRFP/CyO Dfd-YFP* stained for GFP (red), Uninflatable (Uif; white) and Aop (cyan). No specific Aop signals are detected in *aop^{O199}* homozygous embryos (E,F). Sibling embryos homozygous (A,B) or heterozygous (C,D) for the *CyO Dfd-YFP* balancer chromosome were stained in the same reaction and imaged using the same settings as the *aop^{O199}* homozygous embryo. GFP signals in tracheal cells and Dfd-YFP signals in the head region were used to genotype embryos. The protein fragment used to raise the anti-Aop monoclonal antibody (Rebay and Rubin, 1995) includes, but is larger than, the predicted Aop[O199] truncated protein. Thus, lack of Aop staining in *aop^{O199}* embryos could be due to absence of the truncated protein or due to absence of the epitope from the truncated protein. (**G-N**) Stage 12 (G,H), stage 13 (I,J), stage 14 (K,L) and stage 16 (M,N) wild-type embryos expressing *mCherry-NLS* in all tracheal cells were stained for chitin (yellow), mCherry (red) and Aop (cyan). Aop becomes detectable in tracheal cell nuclei at stage 13 (I,J). Aop levels peak at stage 14 (K,L) and subsequently decline to low levels at 16 (M,N). Scale bars: 50 µm.

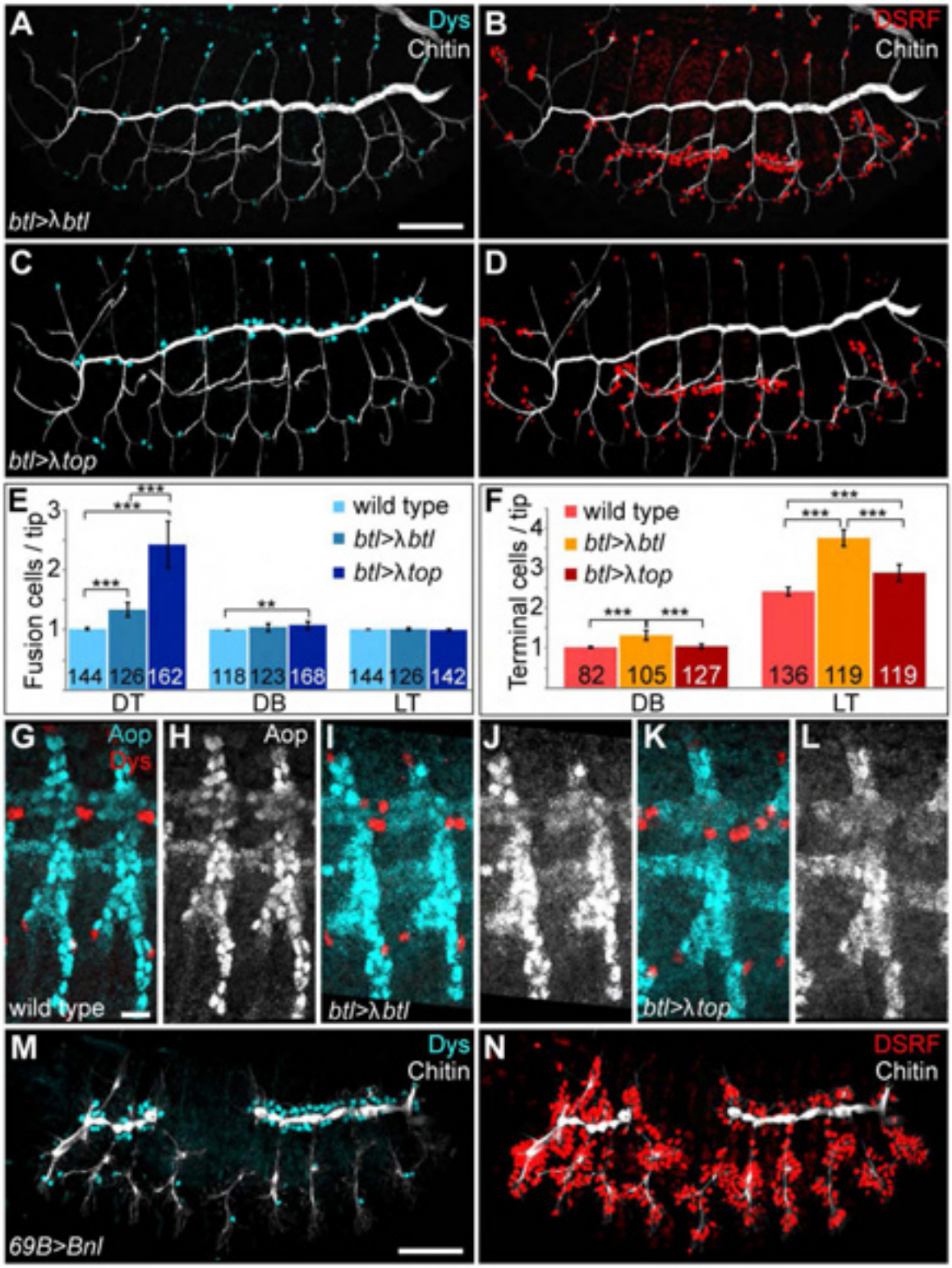

Fig. S3. Effect of constitutively active Receptor Tyrosine Kinase signaling on Aop levels in tracheal cells. (**A-F**) Constitutively active forms of Btl (λBtl; A,B) and EGFR (λTop; C,D) were expressed in tracheal cells under the control of *btl*-Gal4. The two receptors have distinct effects on FC and TC specification, respectively. FCs (E) and TCs (F) were counted in in λBtl- and λTop-expressing embryos. Branch types are indicated below the bars. Numbers inside bars indicate numbers of branch tips scored. Error bars represent s.d. ***$P \leq 0.001$; **$P \leq 0.01$. (**G-L**) Aop protein (cyan) was detected by immunostaining in wild-type embryos (G,H) and in embryos expressing λBtl (I,J) or λTop (K,L). Expression of λBtl and λTop leads to a partial downregulation of Aop in tracheal cells, probably owing to increased degradation (nuclear Aop signals are more diffuse in J and L compared with H). In λTop-expressing embryos (L), nuclear Aop signals in the DT are weaker compared with λBtl-expressing embryos (J), which is consistent with λTop being more potent than λBtl in inducing FCs. (**M**,**N**) Stage 15 embryo overexpressing Bnl in all ectodermal cells using the *69B*-Gal4 driver. Most tracheal cells are mis-specified as DSRF-expressing TCs (red; N), as previously reported, but DT cells are mis-specified mainly as Dys-expressing FCs (cyan; M). Scale bars: 50 µm in A-D,M,N; 10 µm in G-L.

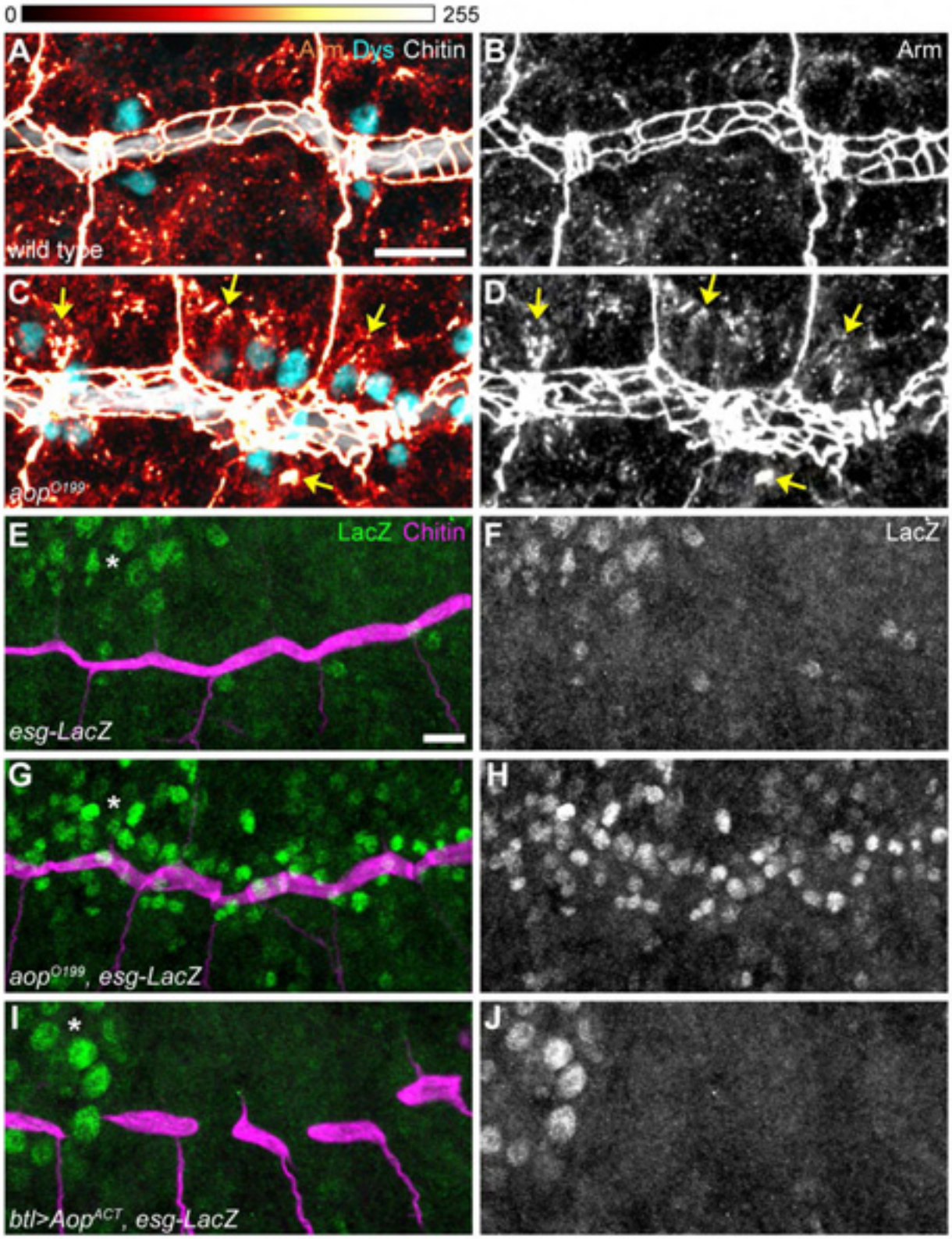

Fig. S4. *aop* mutations lead to accumulation of the Wg signaling effector Arm and to misexpression of the Wg target *escargot.* (**A-D**) Immunostaining showing Armadillo levels in wild-type (A, B) and aop^{O199} mutant embryo (C, D). aop^{O199} embryos show higher levels of intracellular Arm in DT cells compared to wild-type embryos. Also note patches of mislocalized Arm protein in ectopic FCs (C, D, yellow arrows). The images show maximum intensity projections of two sections (ΔZ=1.6 µm). Arm signal intensities in (A and C) are color-coded using a heat map shown on top. Note that Arm signals at AJs are saturated to highlight intracellular Arm signals. (**E-J**) *esg-LacZ* enhancer trap (green in E) reflects Wg-dependent expression of *esg* in two FCs per DT metamere in wild-type embryos (E,F). In aop^{O199} embryos (G,H), *esg-LacZ* is expressed in many more tracheal cells and at higher levels compared with wild-type embryos, consistent with overactivation of Wg signaling. Conversely, *esg-LacZ* is absent from tracheal cells expressing Aop^{ACT} (I,J). Non-tracheal cells expressing *esg-LacZ* are indicated by asterisks in E,G,I. Scale bars: 10 µm.

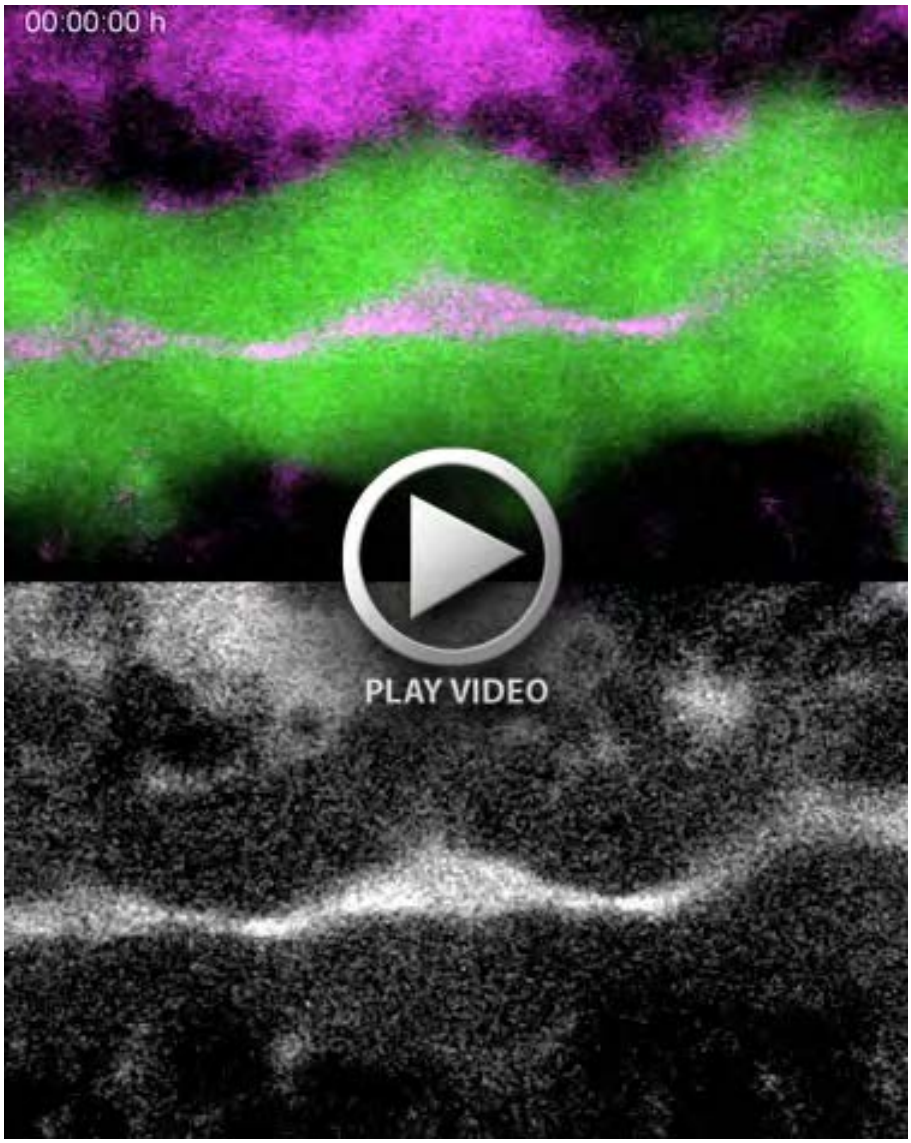

Movie 1. Ectopic tracheal fusion events in an *aop^{O199}* mutant embryo. Time-lapse movie of dorsal trunk in an *aop^{O199}* homozygous mutant embryo expressing GFP (green) and Verm-mRFP (magenta) under the control of *btl*-Gal4. The upper movie shows the merged GFP and Verm-mRFP channels and the lower movie shows the Verm-mRFP channel alone. Two separate cellular inclusions are formed in the DT lumen (green islets inside the lumen) owing to secondary fusion events. The movie was taken with a 40×/1.3 NA lens and a frame rate of 35 seconds. Time is indicated in the top left corner.